Journal of Applied Spectroscopy, Vol. 75, No. 1, 2008

SYNTHESIS OF NANOPARTICLES USING A PULSED ELECTRICAL DISCHARGE IN A LIQUID

V. S. Burakov, N. A. Savastenko,* N. V. Tarasenko, and E. A. Nevar

UDC 533.9;535.343.9

We used a pulsed electrical discharge in a liquid to obtain Cu-, WC-, and ZnO-containing nanoparticles. The effect of the discharge current and pulse duration on the morphology and phase composition of the synthesized material was studied by spectrophotometry, transmission electron microscopy, and x-ray diffraction analysis. We discuss possible mechanisms for nanoparticle formation in a discharge submerged in a liquid.

Key words: *nanoparticle, electrical discharge in a liquid, absorption spectrum, x-ray diffraction analysis.*

Introduction. Development of high-efficiency methods for nanoparticle synthesis has become increasingly important for improving various industrial processes or procedures used, for example, in powder metallurgy or in medicine for precise drug delivery, and also in production of catalysts, dyes, lubricants, etc. Finely dispersed powders of some materials, in particular tungsten carbide, are used in production of cutting and wear-resistant materials [1, 2]. In this case, coatings obtained using powdered materials are generally porous. It is assumed that the presence of nanosized particles in the starting powders substantially reduces the pore size, and that this leads to a significant increase in the hardness of the coatings obtained [3, 4].

Of special interest for medicine are magnetic nanoparticles encapsulated in graphite (amorphous carbon) shells. A graphitic or amorphous carbon shell for nanoparticles on the one hand makes it possible to add substances to the nanoparticle that are to be introduced into the body, and on the other hand provides stability for the nanoparticles in many organic and inorganic liquids as well as biocompatibility for the introduced particles [5]. Encapsulated nanoparticles can also have higher catalytic activity [6, 7]. On the whole, successful application of nanoparticles as catalysts is due to their high surface-to-volume ratio [8]. However, a major change in the physicochemical properties of materials as the characteristic dimensions decrease down to a few or tens of nanometers leads not only to an increase in the total activity of the nanocatalysts but also (which is very important) to a decrease in the temperature range in which high activity of the catalysts is ensured, and a change in their selectivity [9].

Often the composition of dyes includes finely dispersed particles suspended in a liquid vehicle. After drying, a surface colored by such dyes turns out to be coated with particle conglomerates. In some cases, it is desirable for these particles to have certain magnetic properties, in particular ensuring absorption of electromagnetic waves by the dyed surfaces which would make the dyed objects invisible to radar. Nanoparticle are considered promising for use as lubricants [10]. Considerable interest in synthesis of nanoparticles arises in connection with the possibility of using them in microelectronics [11–13]. For successful commercial application of nanoparticles, efficient and low-cost methods for synthesizing them are needed.

In the year 2000, data were published on synthesis of carbon nanotubes in a discharge between two graphite electrodes submerged in liquid nitrogen [14]. At the moment, synthesis of nanoparticles using a pulsed electrical discharge submerged in a liquid is considered as an inexpensive method [14–17]. Since the first publication, many papers have appeared that have been devoted to modification of the method for nanoparticle synthesis in a submerged discharge. It has been suggested that water be used instead of liquid nitrogen as the working liquid [15, 18, 19]. In some cases, nitrogen was passed through the water during the discharge [15]. Arc discharge between nickel, tungsten, steel,

*To whom correspondence should be addressed.

B. I. Stepanov Institute of Physics, National Academy of Sciences of Belarus, 68 prosp. Nezavisimosti, Minsk, 220072, Belarus; e-mail: nataliesavastenko@tut.by. Translated from Zhurnal Prikladnoi Spektroskopii, Vol. 75, No. 1, pp. 111–120, January–February, 2008. Original article submitted November 19, 2007.

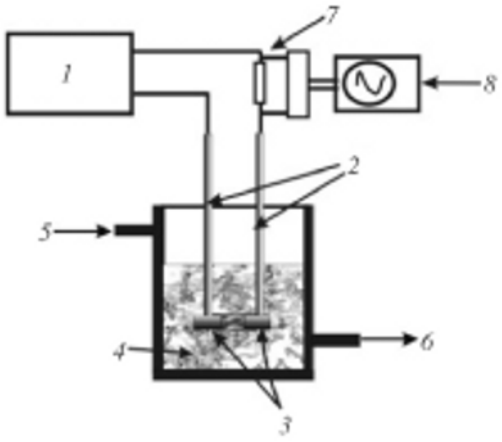

Fig. 1. Block diagram of experimental setup for synthesis of nanoparticles: 1) discharge generator; 2) electrode holders; 3) electrodes; 4) working liquid; 5) and 6) inlet and outlet for liquid in the water cooling system; 7) and 8) resistor and oscillograph for recording the oscilloscope trace of the discharge current.

and graphite electrodes submerged in ethanol has been used for the synthesis. The composition of the particles has been varied from metallic to carbon, including all possible intermediate states [20]. In [21], carbon nanotubes decorated with palladium nanoparticles could be obtained in an arc discharge between two graphite electrodes submerged in a palladium chloride solution. Many publications have been devoted to synthesis of encapsulated nanoparticles (see, for example, [22–27]). Recently it has been demonstrated that it is possible to synthesize metallic Ni, Co, and Fe particles encapsulated in graphite shells, using an arc discharge in aqueous solutions of the following salts of the metals: $NiSO_4$, $CoSO_4$, and $FeSO_4$ [23]. In contrast to the results in [21], the S and O content in the synthesized nanopowder were measured in analysis of the chemical composition.

Despite the large number of papers, there has been no systematic study of the effect of the discharge parameters on the properties of the synthesized material, as is needed to establish the mechanisms for nanoparticle formation during the discharge.

In this work, we have studied the effect of the magnitude of the current and the duration of the discharge on the constituent composition and morphology of nanoparticles synthesized by the pulsed electrical discharge method using copper, tungsten, zinc, and graphite electrodes submerged in a liquid. The absorption spectra were recorded for all the samples. Transmission electron microscopy (TEM) and x-ray diffraction (XRD) were also used to study the nanoparticles.

The Experiment. Figure 1 shows a block diagram of the setup for synthesis of nanoparticles by the submerged discharge method. The setup consists of four basic elements: a discharge generator, electrodes, a glass vessel in which the synthesis is carried out, and a water cooling system. The discharge was created between two electrodes submerged in the liquid to a depth of 3 cm. The synthesis was carried out in 100 mL of liquid. The electrodes were graphite, tungsten, and zinc rods of diameter 6 mm. The cross section of the copper electrode was 2×4 mm. As the working liquid, we used an aqueous solution of $CuCl_2$ with concentration 0.001 M, ethyl alcohol, and distilled water. The optimal distance between electrodes was 0.3 mm. The discharge generator could create ac or dc discharges in "spark" and "arc" modes. A diode bridge was used to obtain dc discharges.

The maximum current for the spark discharge was 60 A, and the duration of the discharge pulse at half-height was 30 μsec. The maximum current and pulse duration of the arc discharge were 10 A and 4 msec. The synthesis was carried out with a voltage of 220 V and 260 V supplied to the electrodes for the ac and dc discharges. The samples were obtained as colloidal solutions of nanoparticles, and as a nanopowder after evaporation of the liquid.

The absorption spectra were recorded using a Cary 500 Scan spectrophotometer in the spectral range 200–800 nm at room temperature, using quartz 50 mm or 100 mm cuvets. To prepare samples for the spectral studies, the synthesis was carried out for 1 min (discharge between copper and graphite electrodes), 30 sec (discharge between tung-

TABLE 1. Nanoparticle Synthesis Conditions and Efficiency

Sample No.	Electrode material	Type, maximum current, duration of discharge	Working liquid	Color of synthesized colloid	Synthesis efficiency, mg/min
1	Cu C	ac spark, 60 A, 30 μsec	Aqueous solution of $CuCl_2$	Yellow	5.9
2	Cu C	ac arc, 10 A, 4 msec	Aqueous solution of $CuCl_2$	Yellow	2.5
3	Cu (cathode) C (anode)	dc spark, 60 A, 30 μsec	Aqueous solution of $CuCl_2$	Brown with Yellowish tinge	2.1
4	Cu (anode) C (cathode)	dc spark, 60 A, 30 μsec	Aqueous solution of $CuCl_2$	Yellow-green (olive)	6.9
5	Cu (cathode) C (anode)	dc arc, 10 A, 4 msec	Aqueous solution of $CuCl_2$	Dark-gray (anthracite)	1.9
6	Cu (anode) C (cathode)	dc arc, 10 A, 4 msec	Aqueous solution of $CuCl_2$	Yellow-green (olive)	3.3
7	W C	ac spark, 60 A, 30 μsec	C_2H_5OH	Black	2.5
8	W C	ac arc, 10 A, 4 msec	C_2H_5OH	Black	0.2
9	W (cathode) C (anode)	dc spark, 60 A, 30 μsec	C_2H_5OH	Black	1.2
10	W (anode) C (cathode)	dc spark, 60 A, 30 μsec	C_2H_5OH	Black	2.1
11	W (cathode) C (anode)	dc arc, 10 A, 4 msec	C_2H_5OH	Black	0.1
12	W (anode) C (cathode)	dc arc, 10 A, 4 msec	C_2H_5OH	Black	0.2
13	Zn Zn	ac spark, 60 A, 30 μsec	H_2O	Gray with blue tinge	40.8
14	Zn Zn	ac arc, 10 A, 4 msec	H_2O	Gray with blue tinge	31.8

sten and graphite electrodes), and 10 sec (discharge between zinc electrodes). A small amount of liquid (5 μL) was deposited via pipet onto a copper mesh for the transmission electron microscope studies. The copper meshes were coated first with a glue composition based on butylacetate ($C_6H_{12}O_2$) and then (after deposition of the sample) by an amorphous carbon film to fix the sample on the glue substrate. The shape and sizes of the synthesized nanoparticles were determined from micrographs obtained on a LEO 906E microscope with operating voltage 120 kV. The nanoparticles obtained were studied by x-ray diffraction in the $2\theta = 15–100^{o}$ region.

The phase composition of the powder was determined by x-ray diffraction on a D8-Advance diffractometer (in CuKα radiation) using the Diffrac Plus EVA software in the PDF-2 card file. To obtain samples for the x-ray diffraction studies, the synthesis was carried out for 10 min. The solution was allowed to stand for some time until a visible precipitate settled on the bottom. This time was about 1 min for samples obtained in a discharge between copper and graphite electrodes, and 3 min for samples obtained in a discharge between zinc electrodes. For samples synthesized in a discharge between tungsten and graphite electrodes, the preliminary sedimentation time was 15 min. Then the colloid was poured into another container, except for the lower 5–8 mL with a large precipitate on the bottom. The colloids synthesized in a discharge between metallic and graphite electrodes were evaporated at room temperature for a

few days to obtain a powder. The evaporation time for the colloids obtained in a discharge between zinc electrodes was a few hours at a temperature of 80°C.

Discussion of Results. We used the submerged discharge method to synthesize Cu-, WC-, and ZnO-containing nanoparticles. 14 samples total were obtained. The experimental conditions for the synthesis are indicated in Table 1.

The discharge was created between the following pairs of electrodes: Cu–C (graphite), W–C (graphite), and Zn–Zn. As the working liquid, we used: an aqueous solution of $CuCl_2$ for synthesis of copper-containing nanoparticles encapsulated in a carbon shell; ethyl alcohol for synthesis of tungsten carbide nanoparticles; water for synthesis of zinc oxide nanoparticles.

The choice of material for the electrodes and surrounding liquid was determined by the need to synthesize nanoparticles of a specific chemical composition. Thus we know [24] that metal-containing nanoparticles encapsulated in graphite shells are formed in a discharge between two graphite electrodes submerged in an aqueous solution of the salts of the corresponding metals. The metallic core of the nanoparticle is formed when the metal ions in solution are reduced during the discharge. The shell of the nanoparticle is formed from atoms vaporized from the surface of the electrodes. In this case, the amount of synthesized material is limited by the salt concentration in solution. In order to eliminate this restriction, we used a discharge between graphite and copper electrodes submerged in an aqueous solution of copper salt ($CuCl_2$). Thus in formation of the metallic core of the particle, not only copper atoms formed as a result of reduction from solution are involved but also atoms entering the discharge zone as a result of erosion of the copper electrode.

For synthesis of tungsten carbide nanoparticles, we used a discharge between tungsten and graphite electrodes placed in ethyl alcohol. The carbon atoms formed on decomposition of the alcohol during the discharge also can participate in formation of the tungsten carbide, thus increasing the efficiency of the nanoparticle synthesis.

As follows from Table 1, the maximum efficiency of the nanopowder synthesis is 6.9 mg/min for a discharge between copper and graphite electrodes, 2.5 mg/min between tungsten and graphite electrodes, and 40.8 mg/min between zinc electrodes. On the whole, the efficiency of nanopowder synthesis is higher in spark discharges than in arc discharges. This rule is followed in the case when metallic (Cu, W) and graphite electrodes are used in both ac and dc discharges for the same polarity of the electrodes. And in both dc spark and arc discharges between metallic and graphite electrodes, the efficiency of the synthesis is higher in cases when a metallic electrode is used as the anode.

The synthesized samples were obtained as colloidal solutions of nanoparticles. In some cases, on the surface of the liquid we observed a floating film, probably consisting of the finest particles. Appreciable settling of the precipitate began 1–15 min after synthesis was finished. Analysis of the data in [20] allows us to hypothesize that the precipitate consists mainly of particles of sizes in the micrometer range. Sometimes on the bottom of the vessel in which the synthesis is carried out, immediately after synthesis is finished we observe large particles most likely formed as a result of decomposition of the electrodes.

Discharge generation in a liquid was accompanied by the process of formation of gas bubbles, consisting of vaporized material from the electrodes and the surrounding liquid. Even 20–30 sec after the start of synthesis, the color of the liquid changed appreciably. The transparency of the liquid gradually decreases. The color of the colloidal solution varied from yellow-green to dark gray when the discharge was generated between graphite and copper electrodes. The yellow-green color of the copper-containing colloidal solutions can arise due to oxidation of the copper [28]. The presence of copper oxides in some of the synthesized colloids was confirmed by x-ray diffraction data (see below), which also suggest that the gray color of the colloid may be explained by the presence of carbon.

The colloidal solutions synthesized in a discharge between tungsten and graphite electrodes were black. The color of the colloids synthesized between metallic and graphite electrodes did not change over time. After evaporation, the color of the powder obtained corresponded to the color of the original colloid. Discharge generation between zinc electrodes led to formation of a black colloid. When the colloid was allowed to stand in air in an open container, it gradually turned milky white.

Figure 2 shows typical absorption spectra for the colloids synthesized in a discharge between copper and graphite electrodes in an aqueous $CuCl_2$ solution, between tungsten and graphite electrodes in ethanol, and between zinc electrodes in water. The colloidal solutions of nanoparticles have pronounced absorption bands or absorb light in a broad spectral region (UV and visible) [29]. The physical reason for absorption of the light are collective coherent oscillations of the electrons, induced on interaction with the electromagnetic field. This phenomenon, known as surface

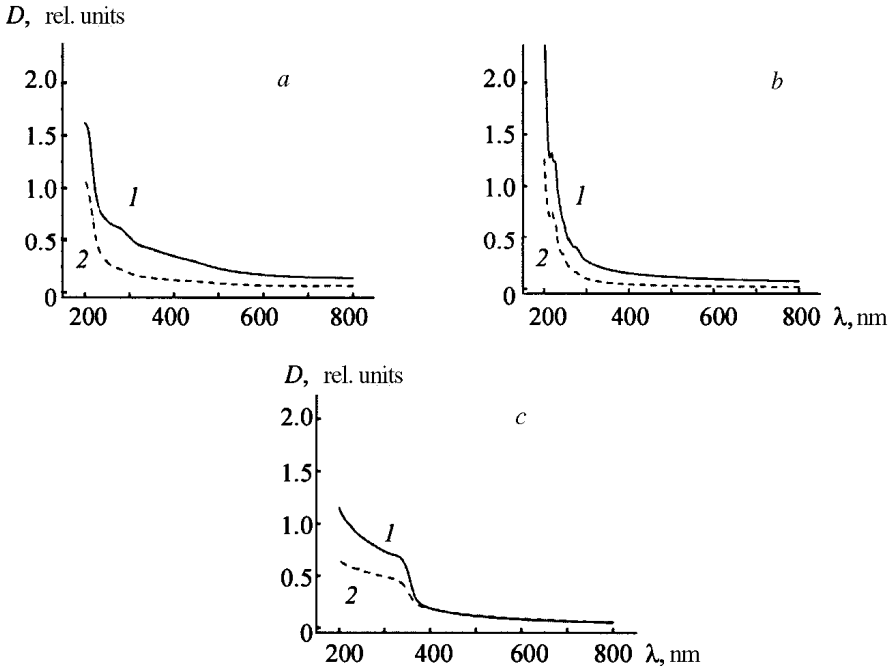

Fig. 2. Absorption spectra of colloidal solutions obtained by using a submerged discharge between copper and graphite electrodes in an aqueous solution of $CuCl_2$ (a), between tungsten and graphite electrodes in ethanol (b), and between zinc electrodes in water (c): 1) spark discharge, 2) arc discharge.

plasmon excitation, is typical for nanoparticles of certain sizes. It is not observed either for individual atoms or for massive material. The position and width of the plasmon resonances depend on the particle sizes, and so recording the absorption spectra of colloidal solutions of nanoparticles is a widely used method for studying nanoparticles in solutions [30].

The optical density of all the synthesized solutions increases as the wavelength decreases (Fig. 2). From comparison of the spectra for colloidal solutions of copper-containing nanoparticles synthesized in ac spark and arc discharges (Fig. 2a, curves 1 and 2), we see that an optically denser solution is synthesized in a spark discharge. The differences in optical density may be connected especially with the different concentrations of nanoparticles in the samples. The efficiency of nanoparticle synthesis in an ac spark discharge is more than twice the efficiency in an ac arc discharge (see Table 1). We also cannot rule out an effect from the constituent composition of the nanoparticles synthesized in spark and arc discharges (see x-ray diffraction data below). In the spectra of samples 1 and 2, there is no absorption peak in the 560–570 nm wavelength region which appears as a result of collective oscillations of electrons in metallic copper particles [31]. The absence of this plasmon peak may be connected, for example, with oxidation of copper particles [32]. This hypothesis with regard to sample 1 was confirmed by the x-ray diffraction data. In the case of sample 2, the absence of plasmon peaks typical of copper is connected with formation of other copper compounds (not oxides). In the spectrum of sample 2, there is a very weak absorption peak with center at $\lambda \approx 289$ nm. This plasmon peak may be connected with the presence of copper nanoparticles of sizes under 4 nm [32, 33]. Although, as shown below, the electron microscope studies confirm the presence of fine particles in the sample, according to x-ray diffraction data there is no copper in sample 1. Most likely secondary products formed during the discharge in the liquid are responsible for absorption in the 289 nm region. Despite observation of copper oxide in the composition of some samples (see x-ray diffraction data), plasmon resonances are not recorded in the 600 nm region associated with the presence of Cu_2O particles [31] in any of the spectra of colloids synthesized in a discharge between copper and graphite electrodes. The absence of this peak may be a consequence of other forms of nanoparticles and their size distributions than in [31].

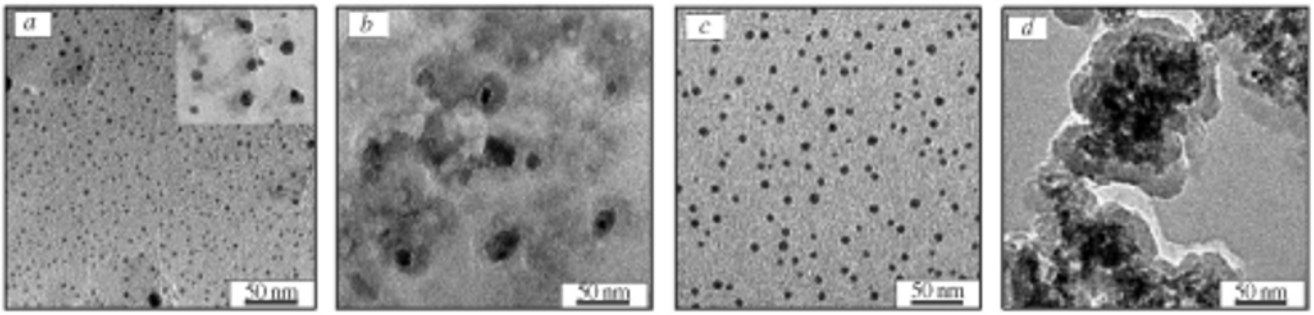

Fig. 3 Typical micrographs of samples synthesized using a submerged discharge between copper and graphite electrodes in spark (a) and arc (b) discharges, and also between tungsten and graphite electrodes in ac spark (c) and arc (d) discharges. Insert: large spherical particles and particles with diffuse edges, also observed in micrographs of sample 1.

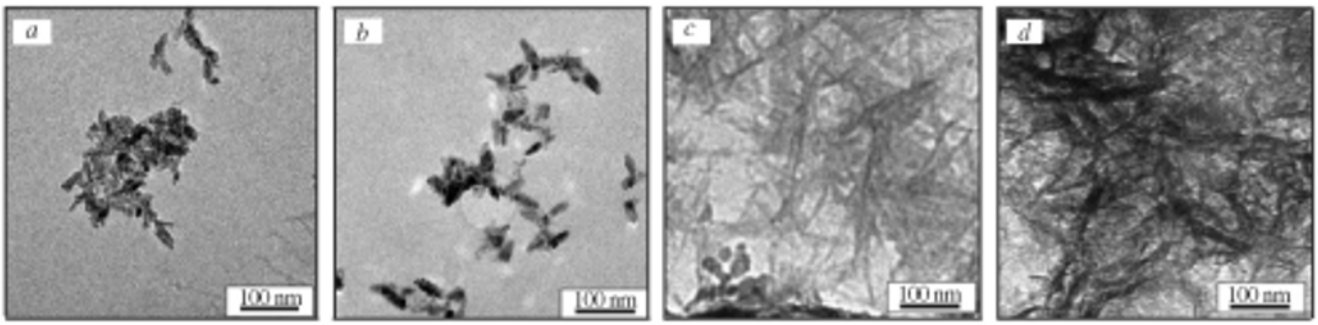

Fig. 4. Micrographs of samples synthesized using a submerged discharge between zinc electrodes in spark (a, c) and arc (b, d) discharges.

As for samples obtained in a discharge between a pair of Cu–C electrodes, the colloid synthesized in an ac spark discharge between W–C electrodes (Fig. 2b, curve 1) has higher optical density than the colloid synthesized in an arc discharge (curve 2). This corresponds to data on the efficiency of nanopowder synthesis (Table 1). Colloid solutions absorb light in the 200–350 nm range. The absorption spectra of the colloids have a weak peak at λ = 220 nm, which is complicated to identify due to the lack of data in the literature.

The colloid synthesized in a spark discharge between two Zn electrodes (Fig. 2c, curve 1) also has higher optical density than the colloid synthesized in an arc discharge (curve 2). In the spectra of both samples, we observe a plateau in the wavelength range 200–375 nm.

TEM was used to study the morphology of the synthesized nanomaterials. Typical micrographs of the samples synthesized in ac spark and arc discharges between metallic (Cu, W) and graphite electrodes are shown in Fig. 3. From comparison of the micrographs for samples obtained in spark and arc discharges, we clearly see that in synthesis in a discharge between a metal-graphite electrode pair, the determining effect on the morphology of the nanoparticles comes from the discharge parameters. In samples synthesized in spark discharges between both a Cu–C and a W–C electrode pair, we observe fine spherical particles (2–7 nm). We should note that on the micrograph of sample 1 (Fig. 3a), synthesized in a spark discharge, larger spherical particles (20 nm or more) are noted as well as formations with diffuse edges (Fig. 3a, insert), also typical of sample 2, synthesized in an arc discharge (Fig. 3b).

For nanoparticles synthesized in ac arc discharges, a core–shell structure is typical (darker regions on the TEM images in Fig. 3b and d: cores surrounded by light gray regions, probably carbon shells). On the micrographs it is quite obvious that it is not individual particles that act as the cores but rather agglomerates of particles. For copper-

TABLE 2 Phase Composition* of Synthesized Nanopowder

Sample No.	Phase (concentration, vol.%)				
1	$Cu_2(OH)_3Cl$ (16.5)	Cu_2OCl_2 (29.7)	C (40.3)	Cu (–)	Cu_2O (13.5)
2	$Cu_2(OH)_3Cl$ (30.0)	Cu_2OCl_2 (5.4)	C (64.6)	Cu (–)	Cu_2O (–)
3	$Cu_2(OH)_3Cl$ (23.9)	Cu_2OCl_2 (–)	C (37.0)	Cu (–)	Cu_2O (39.1)
4	$Cu_2(OH)_3Cl$ (1.4)	Cu_2OCl_2 (–)	C (82.5)	Cu (8.3)	Cu_2O (8.3)
5	$Cu_2(OH)_3Cl$ (33.6)	Cu_2OCl_2 (32.5)	C (33.9)	Cu (–)	Cu_2O (–)
6	$Cu_2(OH)_3Cl$ (15.1)	Cu_2OCl_2 (–)	C (–)	Cu (7.4)	Cu_2O (77.5)
7	W_2C (5.8)	WC_{1-x} (32.8)	C (61.4)	W (–)	W_xO_y (–)
8	W_2C (5.8)	WC_{1-x} (78.1)	C (14.7)	W (–)	W_xO_y (–)
9	W_2C (57.0)	WC_{1-x} (30.7)	C (8.9)	W (3.3)	W_xO_y (–)
10	W_2C (5.6)	WC_{1-x} (32.5)	C (61.8)	W (–)	W_xO_y (–)
11	W_2C (6.2)	WC_{1-x} (90.1)	C (3.7)	W (–)	W_xO_y (–)
12	W_2C (6.6)	WC_{1-x} (71.7)	C (21.9)	W(–)	W_xO_y (–)
13	–	–	–	Zn (35.0)	ZnO (65.0)
14	–	–	–	Zn (31.2)	ZnO (68.2)

*X-ray diffraction data.

containing nanoparticles, the sizes of the cores are no greater than 25 nm, while the particle size in the shell is ≤50 nm (Fig. 3b). WC-containing nanoparticles build up large agglomerates, where core-forming particles form chains a few hundred nanometers long. Despite the fact that the size of the individual nanoparticles in the agglomerates is rather complicated to estimate, comparison of the micrographs shown in Fig. 3a, c and b, d makes it possible to hypothesize that the sizes of single particles making up the core of the structures synthesized in arcs are comparable with the sizes of unagglomerated nanoparticles formed in spark discharges. Core–shell type structures are also observed in dc arc discharges between tungsten and graphite electrodes, and also between copper and graphite electrodes, if a copper electrode is used as the cathode. In the latter case, core–shell structures are observed more rarely than in an ac discharge.

In a dc arc discharge between a copper anode and a graphite cathode, core-shell structures are not observed. As shown by x-ray diffraction, graphite is generally not found in the material synthesized under the given conditions. At the same time, independent of the type of discharge, the material synthesized between tungsten and graphite electrodes always contains graphite.

Based on the above, we can conclude that on the whole, arc discharge conditions are more favorable for the formation of core-shell particles than spark discharge conditions. However, the process of forming such structures is accompanied by a chain of chemical reactions, the result of which may be a deficiency of the material needed for shell formation.

The morphology of the nanoparticles is determined not only by the discharge parameters but also by their chemical composition. While the nanoparticles containing copper and tungsten carbide have mainly a spherical shape, the ZnO-containing nanoparticles are needle-shaped or ellipsoidal (Fig. 4). Figure 4 shows typical micrographs of samples obtained in spark and arc discharges between two zinc electrodes submerged in water. We see that the studied material consists mainly of needle-shaped formations. The lengths of the individual "needles" reaches 150–200 nm for a width of 10–15 nm. We also observe ellipsoidal nanoparticles. The sizes of the individual particles are difficult to exactly determine due to agglomeration. According to our estimates, the linear dimensions of the individual ellipsoidal nanoparticles can be estimated as falling within the range 8–15 nm (width) and 40–50 nm (length).

We should point out that formation of both needle-shaped and ellipsoidal structures occurs in both a spark and an arc discharge. Most likely the morphology of nanostructures obtained by the method of a discharge between two identical metallic electrodes submerged in a liquid does not depend on the discharge parameters.

The x-ray diffraction results for the synthesized material are shown in Table 2. X-ray phase analysis (i.e., identification of the qualitative composition and semiquantitative determination of the components in the sample) was

carried out based on analysis of the dependence of the scattered x-ray intensity on the scattering angle. The presence of sharp peaks on the x-ray diffraction patterns is usually connected with a crystal structure in the samples. Amorphous structure is apparent in broad peaks in the regions typical of the studied material [34, 35]. Pronounced peaks were detected on the x-ray diffraction patterns of samples 1–6. The diffraction peaks corresponding to $2\theta = 43.2$ and 50.3^{o} suggest the presence of metallic copper with a face-centered cubic lattice. The three diffraction peaks with $2\theta = 36.5$, 42.3, and 61.4^{o} may be assigned to copper oxide Cu_2O with a primitive cubic lattice. The two peaks near $2\theta = 24.0$ and 26.5^{o} indicate that hexagonal carbon is present in the samples. According to [31], amorphous carbon appears as strongly broadened peaks in the regions $2\theta = 20–30^{o}$ and $2\theta = 40–50^{o}$. Analysis of the diffraction patterns shows that no amorphous carbon is present in the synthesized samples. Furthermore, x-ray diffraction revealed formation of two more copper and chlorine compounds: $Cu_2(OH_3)Cl$ (monoclinic lattice, $2\theta = 16.5$, 19.0, 31.0, 32.3, 32.7, 33.0, 38.7, 39.8, 40.1, 50.3, 50.5, 53.8^{o}), Cu_2OCl_2 (orthorhombic lattice, $2\theta = 17.8$ and 36.0^{o}). Peaks corresponding to $CuCl_2$ were not detected on the diffraction patterns of the synthesized samples.

The samples obtained in a discharge between tungsten and graphite electrodes are a mixture of W_2C (hexagonal lattice, diffraction peaks correspond to $2\theta = 34.7$, 38.2, 39.8, 52.3, 62.1, 69.9, 75.0^{o}), WC_{1-x} (face-centered cubic lattice, $2\theta = 36.8$, 42.8, 62.0, 74.1, 78.1^{o}), C (hexagonal lattice, $2\theta = 26.5^{o}$), and a small amount of W (body-centered cubic lattice, $2\theta = 40.3^{o}$). No amorphous graphite or tungsten oxides (W_xO_y) were observed.

On the diffraction patterns of samples synthesized in a discharge between zinc electrodes, we observe only peaks corresponding to ZnO (hexagonal lattice, $2\theta = 32.1$, 34.6, 36.7, 47.9, 57.2, 63.1, 67.1, 68.6, 69.8^{o}) and Zn (hexagonal lattice, $2\theta = 36.3$, 39.0, 43.2, 54.2, 70.0, 70.8, 82.0, 86.5^{o}).

As we see from Table 2, the percent ratio of the different components in the samples synthesized in discharges between metallic (Cu, W) and graphite electrodes depends to a significant extent on the discharge parameters: maximum discharge current, discharge pulse duration, and also (in the case of generation of dc discharges) the polarity of the electrodes. Copper nanoparticles are found only in samples obtained in dc discharges with a copper anode. Mainly copper enters into the composition of the synthesized nanopowder in the form of the oxide (Cu_2O), the hydroxychloride ($Cu_2(OH_3)Cl$), and the oxychloride (Cu_2OCl_2). The difference between our data and the results of [21], which reported the absence of chlorine in the composition of material synthesized in a discharge submerged in a $PdCl_2$ solution, is due most likely to the different chemical properties of Cu and Pd, in particular their ability to form a chemical compound with chlorine. Metallic tungsten is found only in the nanopowder synthesized in a dc spark with a tungsten cathode. Depending on the discharge regime, tungsten carbides (W_2C and WC_{1-x}) make up ≈40–90 vol.% of the synthesized nanopowder.

The copper oxide content in samples obtained using a pair of Cu–C electrodes varies over a broad range (0–80 vol.%). When the nanopowder is synthesized in a discharge between a pair of W–C electrodes, no tungsten oxides are observed. The carbon content in samples synthesized in discharges both between Cu–C electrodes and between W–C electrodes also varies considerably (0–80 vol.%). However, despite the fact that variation in the carbon content was observed within the same limits for samples synthesized using both Cu–C and W–C electrodes, no general trend was revealed in the effect of the discharge parameters on the carbon concentration.

Obviously the constituent composition of the nanopowder is determined to a quite considerable extent by the reactivity of the chemical elements entering into the composition of the electrodes and the surrounding liquid. (For example, in contrast to tungsten, copper is readily oxidized but does not form carbides.) So study of the effect of the discharge parameters on the constituent composition of the synthesized nanoparticles is advisable only for identical pairs of electrodes.

Taking the above into account, we can conclude that for synthesis of copper oxide Cu_2O and tungsten carbide WC_{1-x} particles used as catalysts [36, 37], the most suitable type of discharge is a dc arc with a copper anode and a graphite cathode, and a dc arc with tungsten cathode and graphite anode.

The constituent composition of samples synthesized in discharges between two identical metallic electrodes remains practically unchanged as the magnitude of the current and the pulse duration of the discharge are varied. The ratio ZnO:Zn in all the synthesized samples was ≈2:1.

Although up to now no direct experimental evidence has been obtained indicating a specific mechanism for the formation of nanoparticles in a discharge submerged in a liquid, we can hypothesize that the following processes occur during the discharge.

During the discharge, the electrodes are heated, melted, and vaporized. Near the elecrodes, the liquid is also vaporized as a result of exposure to high temperature. According to estimates in [19], the temperature in the discharge zone varies approximately from the boiling point of the electrode material near the electrodes to the boiling point of the liquid at the gas mixture-liquid boundary. Thus in the discharge zone between copper and graphite electrodes in water, the range of variation in the temperatures should be 4000 to 100°C (the melting points and boiling points of graphite and copper are 3527°C, 4027°C and 1085°C, 2562°C respectively). The discharge occurs in a gas mixture consisting of the vapor of the working liquid and the electrode materials, with a high temperature gradient. If even one of the electrodes contains carbon, then the gas mixture can contain CO and H_2, formed as a result of the reaction [19]:

$$C + H_2O \rightarrow CO + H_2 \quad (1)$$

In some cases, reaction (1) can lead to complete disappearance of water vapor from the discharge zone [19]. In the case of a discharge between copper and graphite electrodes, the copper vapor can enter the discharge zone both as a result of erosion of the electrode and as a result of vaporization and thermal decomposition of the working liquid (aqueous solution of $CuCl_2$). In the latter case, chlorine should also be separated. Nanoparticles are formed in the gas mixture as a result of the sequential change from nucleation to growth to coalescence to aggregation. The growth of nanoparticles stops as a result of interaction with the colder liquid surrounding the discharge zone. The presence of water vapor in the mixture leads to the appearance of oxides, which then can be reduced as a result of reactions with CO and H_2:

$$Cu_2O + CO \rightarrow 2Cu + CO_2 \quad (2)$$

$$Cu_2O + H_2 \rightarrow 2Cu + H_2O \quad (3)$$

However, as follows from x-ray diffraction data, reduction of copper oxide occurs only partially in some types of discharge. The determining steps are reactions with chlorine, leading to formation of copper hydroxychloride ($Cu_2(OH)_3Cl$) and copper oxychloride (Cu_2OCl_2). No copper carbide is observed, since copper does not react with carbon even at high temperatures [38].

In the case of a discharge between tungsten and graphite electrodes, the temperature in the discharge zone varies from ≈5500°C to 80°C (the melting point and boiling point of tungsten are 3422°C and 5555°C, the boiling point of alcohol is 78°C). In the gas mixture formed near the electrodes, during the discharge we find not only vaporized electrode material but also thermal decomposition products of ethanol.

With thermal decomposition of ethanol occurring with dissociation of C–C or C–O bonds, both stable products such as H_2O, C_2H_4, CH_4, CH_3COH, CH_2O, etc. and radicals (including CH_3) can be formed, which then react with the ethanol and its decomposition products, participating in chain reactions [39–41].

According to data in [39], at temperatures below 2500°C and a pressure <10 atm, the most likely thermal decomposition products of ethanol are C_2H_4 and H_2O, formed according to the following scheme:

$$C_2H_5OH \rightarrow C_2H_4 + H_2O \quad (4)$$

Since near the electrodes a region is formed with a temperature gradient, we should expect the existence of other decomposition products of ethanol (all the way down to atomic C, H, and O), nonuniformly distributed in the discharge zone. The hydrocarbons and carbon formed react with tungsten, forming carbides (W_2C and WC) [42, 43].

In the traditional method for obtaining carbides, a mixture of tungsten (or its oxide) and carbon is calcined at a temperature of 1400°C–1800°C for a few hours [43, 45]. The reaction is solid-state and is limited by the diffusion rate. The reaction time can be significantly shortened by using hydrocarbons as the carbon source [44, 45]. In this case, the reaction occurs in the gas-solid system, which provides the best contact between reagents and consequently a decrease in the reaction time down to 2 h and a decrease in temperature down to 850°C [44]. Under the conditions for a discharge in a liquid, carbides are formed during a few milliseconds as a result of gas-phase reactions. For example, we know that tungsten dimers react with C_2H_4 even at room temperature, and so reactions of carbide formation can occur over the entire discharge zone [46].

The temperature in the discharge zone between zinc electrodes is no higher than 900°C (the boiling point of zinc is 907°C). A freshly prepared colloidal solution was black, which gradually turned to milky white. Since we know that zinc does not react with water, we should hypothesize that zinc nanoparticles were formed in the discharge which, by reacting with oxygen dissolved in the liquid, form zinc oxide (white powder):

$$2Zn + O_2 \rightarrow 2ZnO \quad (5)$$

Reaction (5) can also occur after vaporization of the working liquid between unoxidized zinc nanoparticles and oxygen from the air. The proposed mechanism for the formation of ZnO nanostructures allows us to explain not only the change in color of the colloid during evaporation, but also the x-ray diffraction data. A change in the discharge parameters does not have an effect on the ZnO:Zn ratio in the synthesized material, since ZnO is formed after the discharge is finished and is determined by heterogeneous reactions with oxygen contained in the working liquid or in the surrounding atmosphere.

Conclusion. Analysis of the results obtained showed that using a pulsed electrical discharge in a liquid provides broad opportunities for synthesis of nanostructures with specified physicochemical properties. We used the method of a pulsed electrical discharge in a liquid to synthesize Cu- and WC-containing nanoparticles of spherical shape and minimum diameter 2 nm, and also needle-shaped structures of length up to 200 nm and width up to 15 nm and ellipsoidal structures of length up to 50 nm and width up to 15 nm, containing ZnO.

The morphology and constituent composition of the synthesized nanoparticles can be modified by changing the magnitude of the current and the pulse duration of the discharge, if for the synthesis we use a discharge between one metallic and one graphite electrode. In discharges with maximum current 10 A and duration 4 msec, conditions are created that promote formation of core-shell type nanoparticles. The morphology and constituent composition of nanoparticles synthesized between two zinc electrodes do not change as the current is varied from 60 A to 10 A and the pulse duration is varied from 30 msec to 4 msec.

This work was done within a project of the Belorussian Republic Foundation for Basic Research (project F06MS-023, "Synthesis of nanosized structures of metals and their compounds by the method of electrical erosion in liquid media"), the Nanomaterials and Nanotechnology Task of the State Comprehensive Program for Scientific Research, and also with the financial support of the state program on "New high-efficiency technologies and equipment for synthesis and processing of materials using concentrated energy fluxes, nuclear and radiation treatment" of the State Program for Preliminary Basic Research.

REFERENCES

1. K. J. Brookes, *World Directory and Handbook of Hardmetals and Hard Materials*, International Carbide Data, Hertfordshire UK (1992), p. 88.
2. P. Ettmayer, *Ann. Rev. Mater. Sci.*, **19**, 145–164 (1989).
3. C. J. Terry and J. D. Frank, "Monocrystalline tungsten monocarbide powder and process for producing," US Patent 4,834,963 (1989).
4. W. D. Schubert, H. Neumeister, and G. Kinger, *Int. J. Ref. Metals Hard Mat*., **16**, 133–142 (1998).
5. M. Bystrzejewski, A. Huczko, and H. Lange, *Sensors and Actuators B*, **109**, 81–85 (2005).
6. M. Manzoli and F. Boccuzzi, *J. Power Sources*, **145**, 161–168 (2005).
7. T. Moon, C. Kim, S.-T. Hwang, and B. Park, *Electron. Solid-State Lett*., **9**, A408–A411 (2006).
8. U. Heiz, S. Abbert, H. Hakkinen, and U. Landman, *Mat. Res. Soc. Symp. Proc*., **648** P9.1.1–P9.1.10 (2001).
9. N. Savastenko, H.-R. Volpp, O. Gerlach, and W. Strehlau, *J. Nanopart. Res*. (in press).
10. L. Rapoport, Y. Bilik, Y. Feldman, M. Hamyonfe, S. R. Cohen, and R. Tenne, *Nature*, **387(6635)**, 791–793 (1997).
11. S. W. Chung, J.-X. Yu, and J. R. Heath, *Appl. Phys. Lett*., **76**, 2068–2070 (2000).
12. Y. Cui, X. Duan, J. Hu, and C. M. Lieber, *J. Phys. Chem. B*, **104**, 5213–5216 (2000).
13. Y. Cui and C. M. Lieber, *Science*, **291**, 851–853 (2001).
14. M. Ishigami, J. Cummings, A. Zettl, and S. Chen, *Chem. Phys. Lett*., **319**, 457–459 (2000).
15. N. Sano, *J. Phys. D*, **37**, L17–L20 (2004).

16. N. Sano, T. Kikuchi, H. Wang, M. Chhowalla, and G. A. J. Amaratunga, *Carbon*, **42**, 95–99 (2004).
17. N. Sano, J. Nakano, and T. Kanki, *Carbon*, **42**, 686–688 (2004).
18. N. Sano, H. Wang, I. Alexandrou, M. Chhowalla, and G. A. J. Amaratunga, *J. Nature* (London), **414**, 506–507 (2001).
19. N. Sano, H. Wang, I. Alexandrou, M. Chhowalla, K. B. K. Teo, G. A. J. Amaratunga, and K. J. Jimura, *Appl. Phys.*, **92**, 2783–2788 (2002).
20. N. Parkansky, B. Iterkop, R. L. Oxman, S. Oldsmith, Z. Arkay, and Y. Lereah, *Powder Technology*, **150**, 36–41 (2005).
21. D. Bera, S. C. Kuiry, M. McCutchen, and S. Seal, *J. Appl. Phys.*, **96**, 5152–5157 (2004).
22. Y. L. Hsin, K. C. Hwang, R.-R. Chen, and J. Kay, *J. Adv. Mater.*, **13**, 830–833 (2001).
23. B. Xu, J. Guo, X. Wang, X. Liu, and H. Ichinose, *Carbon*, **44**, 2631–2634 (2006).
24. X. Lange, M. Sioda, A. Huezko, Y. Q. Zhu, H. W. Kroto, and D. R. M. Walton, *Carbon*, **41**, 1617–1623 (2003).
25. K. H. Ang, I. Alexandrou, N. D. Mathur, G. A. J. Amaratunga, and S. Hag, *Nanotechnology*, **15**, 520–524 (2004).
26. J. S. Qui, Y. F. Li, Y. P. Wang, Z. B. Zhao, and Y. G. Wang, *Fuel*, **83**, 615–617 (2004).
27. D. Bera, S. C. Kuiry, M. McCutchen, A. Kruize, H. Heinrich, M. Meyyappan, and S. Seal, *Chem. Phys. Lett.*, **386**, 364–368 (2004).
28. M.-S. Yeh, Y.-S. Yang, Y.-P. Lee, Y.-H. Yeh, and C.-S. Yeh, *J. Phys. Chem. B*, **103**, 6851–6857 (1999).
29. C. Burda, T. Green, C. Landes, S. Link, R. Little, J. Petroski, and M. A. El-Sayed, in: Zhong Lin Wang, ed., *Characterization of Nanophase Materials*, Wiley-VCH (2000).
30. J. Wang, H. F. M. Boelens, M. B. Thathagar, and G. Rothenberg, *Chem. Phys. Chem.*, **5**, 93–98 (2004).
31. A. Yanase and H. Komiyama, *Surf. Sci.*, **248**, 11–19 (1991).
32. M. Aslam, G. Gopakumar, T. L. Shoba, I. S. Mulla, and K. J. Vijayamohanan, *Colloid. Inter. Sci.*, **255**, 79–90 (2002).
33. R. A. Salkar, P. Jeevanandam, G. Kataby, S. T. Aruna, Y. Koltypin, O. Palchik, and A. Gedanken, *J. Phys. Chem. B*, **104**, 893–897 (2000).
34. M. B. Zellner and J. G. Chen, *Catal. Today*, **99**, 299–307 (2005).
35. S. I. Drapak, A. P. Bakhtinov, S. V. Gavrilyuk, Yu. I. Prilutskii, and Z. D. Kovalyuk, *Fiz. Tverd. Tela*, **48**, 1515–1517 (2006).
36. V. S. Burakov, A. V. Butsen, V. Bruser, F. Harnisch, P. Ya. Misakov, E. A. Nevar, M. Rosenbaum, N. A. Savastenko, and N. V. Tarasenko, *J. Nanopart. Res.* (in press).
37. V. S. Burakov, A. V. Butsen, P. Ya. Misakov, A. A. Nevar, V. Z. Radkevich, N. A. Savastenko, and N. V. Tarasenko, in: *Proceedings, Twenty-Eighth International Conference on Phenomena in Ionized Gases (ICPIG)*, Prague, Czech Republic (2007), pp. 637–640.
38. Chemical Encyclopedia, *Sov. Entsikl.*, Moscow (1961), Vol. 3, p. 78.
39. J. Park, R. S. Zhu, and M. C. J. Lin, *J. Chem. Phys.*, **117**, 3224–3231 (2002).
40. Z. F. Hu, J. Park, and M. C. Lin, *J. Chem. Phys.*, **120**, 6593–6598 (2004).
41. J. Li, A. Kazakov, and F. L. Dryer, *J. Phys. Chem. A*, **108**, 7671–7680 (2004).
42. Chemical Encyclopedia, *Sov. Entsikl.*, Moscow (1961), Vol. 1, p. 651.
43. C. J. Smithells, *Tungsten* [Russian translation], GNTI po Chern. i Tsv. Metallurgii, Moscow (1958).
44. F. F. P. Medeiros, S. A. De Oliveira, C. P. De Souza, A. G. P. Da Silva, U. U. Gomes, and J. F. De Souza, *Mater. Sci. Engineer.*, **A315**, 58–62 (2001).
45. A. Lackner and A. Filzweiser, "Gas carburizing of tungsten carbide (WC) powder," US Patent 6447442 (2002).
46. Y. Ishikawa and Y. Matsumoto, *Chem. Phys. Lett.*, **352**, 209–212 (2002).